Annu. Rev. Earth. Planet. Sci. 1999. 27:287–312

KUIPER BELT OBJECTS

David Jewitt
Institute for Astronomy, 2680 Woodlawn Drive, Honolulu, HI 96822;
e-mail: jewitt@ifa.hawaii.edu

KEY WORDS: Neptune, Pluto, planet formation, outer solar system, short-period comets

ABSTRACT

The region of the solar system immediately beyond Neptune's orbit is densely populated with small bodies. This region, known as the Kuiper Belt, consists of objects that may predate Neptune, the orbits of which provide a fossil record of processes operative in the young solar system. The Kuiper Belt contains some of the Solar System's most primitive, least thermally processed matter. It is probably the source of the short-period comets and Centaurs, and may also supply collisionally generated interplanetary dust. I discuss the properties of the Kuiper Belt and provide an overview of the outstanding scientific issues.

HISTORY OF THE KUIPER BELT

Edgeworth (1943) was the first to speculate on the existence of planetary material beyond the orbit of Pluto. Referring to the solar nebula, he wrote, "It is not to be supposed that the cloud of scattered material which ultimately condensed to form the solar system was bounded by the present orbit of the planet Pluto; it is evident that it must have extended to much greater distances." He also suggested that the trans-Plutonian region was the repository of the comets: "From time to time a member of this swarm of potential comets wanders from its own sphere and appears as an occasional visitor to the inner regions of the solar system." These qualitative ideas were later repeated by Edgeworth (1949) and echoed by Kuiper (1951), who gave no indication that he was aware of Edgeworth's papers. Rather, his motivation was in part to correct Oort's (1950) assertion that the comets formed near, and were ejected by, Jupiter and had a composition like that of the main-belt asteroids. Edgeworth's and Kuiper's remarks were purely speculative rather than predictions in the

0084-6597/99/0515-0287$08.00

accepted, scientific sense. Perhaps for this reason, the notion of a trans-Neptunian belt had a less immediate impact on the subsequent development of cometary science than did the contemporaneous but more quantitative work by Oort (1950) and Whipple (1951). Nevertheless, the possibility of a trans-Plutonian ring was clearly recognized before the middle of the 20th century. This concept was sustained by Whipple (1964) and others, while much later Fernandez (1980) explicitly re-proposed a trans-Neptunian ring as a source of the short-period comets.

Baum & Martin (1985) suggested (but apparently did not attempt) an early observational test of the comet belt hypothesis. Luu & Jewitt (1988) made a concerted but ultimately unsuccessful observational effort in which both photographic plates and an early charge-coupled device (CCD) were used to examine the ecliptic. In the same year, Duncan, Quinn, & Tremaine (1988) provided additional motivation for searches by showing that a flattened, disk-like source was required to fit the restricted range of inclinations of the short-period comets. Further ecliptic surveys by Kowal (1989), Levison & Duncan (1990), Cochran et al (1991) and Tyson et al (1992) proved negative. Observational success was achieved first with the discovery of 1992 QB1 (Jewitt & Luu 1993) and followed up with the rapid discovery of a growing number of trans-Neptunian bodies (Jewitt & Luu 1995, Irwin et al 1995, Williams et al 1995, Jewitt et al 1996, Luu et al 1997, Jewitt et al 1998, Gladman et al 1998). These discoveries have powered a veritable explosion of research on the Kuiper Belt in the past half decade. Indeed, Pluto itself is now considered to be the largest known Kuiper Belt Object.

The purpose of this review is to summarize the current observational constraints on the Kuiper Belt, and to discuss extant models and theories of its formation and evolution, all in a style suited to the diverse readership of the *Annual Review of Earth and Planetary Sciences*. The known population of the Kuiper Belt, as well as the important literature on this subject, changes on short timescales compared to the interval between reviews such as this. For the most recent information, the reader is referred to a list of orbital parameters maintained by Brian Marsden and Gareth Williams (http://cfa-www.harvard.edu/cfa/ps/lists/TNOs.html) and to a general site covering the Kuiper Belt maintained by the author (http://www.ifa.hawaii.edu/faculty/jewitt/kb.html).

OBSERVING THE KUIPER BELT

Kuiper Belt objects (KBOs) are best identified by their slow, retrograde (westward) motions when observed in the anti-solar direction. Then, the angular velocity, $d\theta/dt$ [arcsec hr^{-1}] is determined largely by parallax. Slow speeds

indicate large distances, according to

$$d\theta/dt \approx \frac{148}{R + R^{1/2}} \tag{1}$$

where R[AU] is the heliocentric distance, and the geocentric distance is taken as $\Delta = R - 1$. The apparent red magnitude m_R, of an object observed in reflected light is given by

$$p_R r^2 \phi(\alpha) = 2.25 \times 10^{16} R^2 \Delta^2 10^{0.4(m_\odot - m_R)} \tag{2}$$

in which p_R is the geometric albedo, r[km] is the object radius, $\phi(\alpha)$ is the phase function and $m_\odot$ is the apparent magnitude of the sun (Russell 1916). At opposition we may take $\phi(0) = 1$. Equations 1 and 2 are plotted in Figure 1, assuming $p_R = 0.04$. The figure shows that 100 km sized objects beyond Neptune should exhibit apparent red magnitudes greater than 22 and characteristic slow retrograde motions (a few arcsec per hour). Successful Kuiper Belt

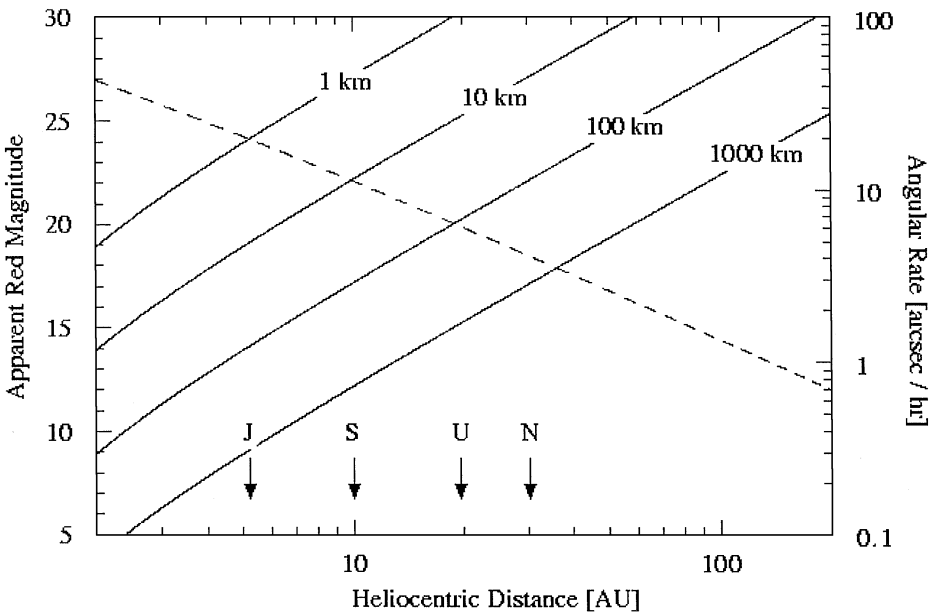

Figure 1 Apparent red magnitude (*left*) and retrograde opposition angular rate (*right*) of KBOs as a function of distance from the sun. Magnitudes were computed from Equation 2 assuming geometric albedo 0.04, radii as marked on the figure and observation at opposition (phase function = 1 and $\Delta = R - 1$). The angular rate is computed from Equation 1 (*dashed curve*). The locations of the major planets are indicated.

surveys have therefore been designed to reveal faint objects moving slowly with respect to the background stars. Increasingly, these surveys are automated (Trujillo & Jewitt 1998) so as to accommodate large data rates.

CONTENTS OF THE KUIPER BELT

At the time of writing (August 1998), ground-based surveys have revealed 69 KBOs, of which 43 possess relatively reliable multi-opposition orbits. The orbits of known KBOs naturally divide into three distinct categories.

Classical Objects

About two thirds of the observed KBOs have semi-major axes $42 \leq a \leq 47$ AU, and seem unassociated with resonances (Figures 2 and 3). These objects define

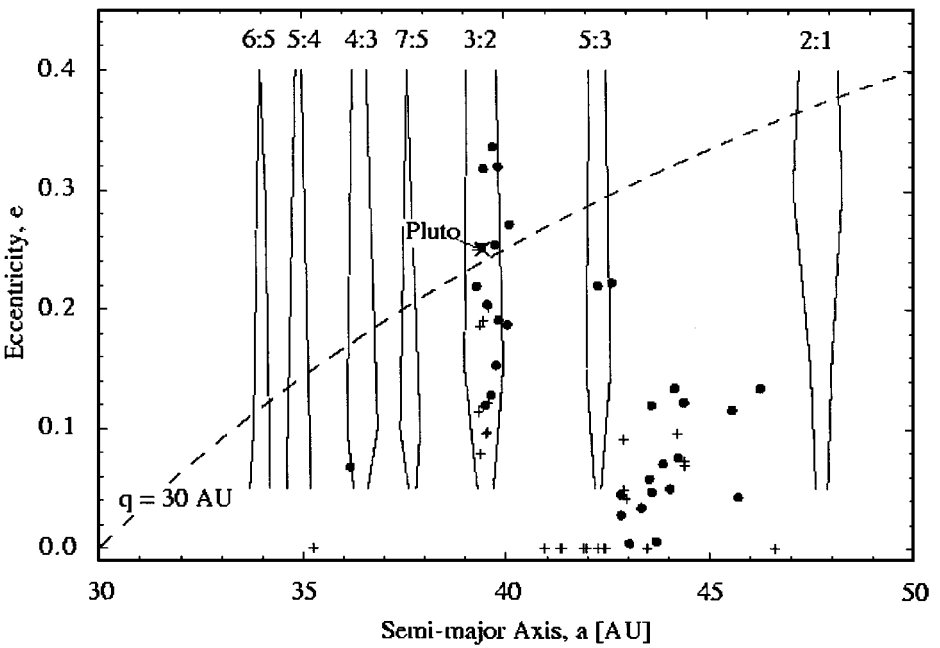

Figure 2 Semi-major axis versus orbital eccentricity for the known KBOs. Multi-opposition objects (*solid circles*) are distinguished from single-opposition objects (*pluses*) and Pluto (*cross*). The distribution is highly nonrandom and shows a clear correlation with mean motion resonances (approximate boundaries of these resonances are shown as *vertical bands*, taken from Malhotra 1995). The *diagonal dashed line* separates objects having perihelion inside Neptune's orbit (above the line) from those wholly exterior to that planet (below the line). Scattered KBO 1996 TL66 falls outside and is omitted from the plot.

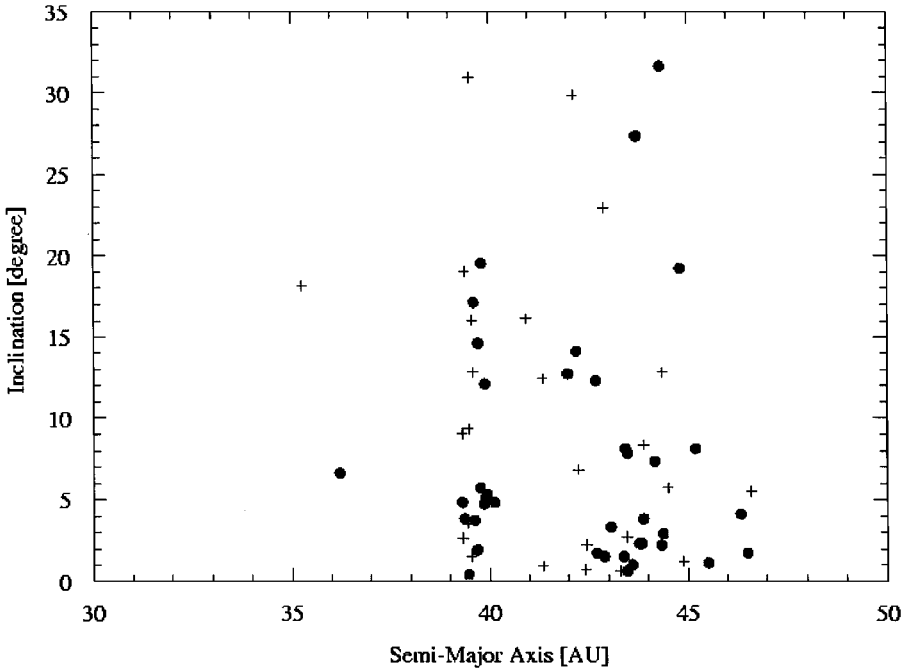

Figure 3 Distribution of semi-major axis versus orbital inclination for the known KBOs. Multi-opposition objects (*solid circles*) are distinguished from single opposition objects (*pluses*). Scattered KBO 1996 TL66 is omitted from the plot.

the "classical" Kuiper Belt. Classical KBOs have small eccentricities (median $e = 0.07$) that maintain a large separation (mostly >10 AU) from Neptune even when at perihelion. The inclinations occupy a wide range ($0 \leq i \leq 32^\circ$).

Resonant Objects (Plutinos)

About one third of the known objects reside in the 3:2 mean motion resonance with Neptune at $a = 39.4$ AU (Figures 2 and 3). These bodies are collectively known as Plutinos ("little Plutos") to highlight the dynamical similarity with Pluto, which also resides in this resonance (Malhotra & Williams 1998). The apparent abundance of the Plutinos is affected by observational bias. Corrected for their smaller mean heliocentric distance (relative to classical KBOs), they probably constitute 10 to 15 percent of the population inside 50 AU (Jewitt et al 1998). The eccentricities ($0.1 \leq e \leq 0.34$) and inclinations ($0 \leq i \leq 20^\circ$) of the Plutinos bracket the values of Pluto ($e = 0.25, i = 17^\circ$). Presumably, the resonance provides immunity to destabilizing perturbations from Neptune.

Indeed, some of the Plutinos have perihelia inside Neptune's orbit (as does Pluto) and would be immediately ejected if not for the protection offered by the resonance. Other resonances (notably the 4:3 and the 5:3) may also be populated, although at a lower level than the 3:2. No objects have yet been found in the 2:1 resonance.

Scattered Objects

The observational sample includes one clearly deviant object, 1996 TL66 (a,e,i = 85 AU, 0.59, 24°; Luu et al 1997). The proximity of the perihelion (q = 35 AU) to Neptune (at 30 AU) suggests a weak dynamical involvement with that planet. It is likely that 1996 TL66 is the first detected member of a population of bodies scattered by Neptune (Fernandez & Ip 1983) and having dynamical lifetimes measured in billions of years (Duncan & Levison 1997). Such scattered KBOs may occasionally enter the planetary system, constituting a source of short-period comets separate from that of chaotic zones.

MODELS

Models of the Kuiper Belt have evolved in a somewhat piece-meal fashion. Most published dynamical models neglect mutual gravitational interactions and collisions among KBOs. This is reasonable in the present-day, low-density Kuiper Belt (but see Ip & Fernandez 1997). However, several lines of evidence now point to the existence of a once more massive Kuiper Belt, in which mutual interactions may have excited a collective (wave) response to perturbations (Ward & Hahn 1998) and in which collisions played an important role. Accordingly, models describing collisions have recently appeared (Farinella & Davis 1996, Stern & Colwell 1997), but have not yet been integrated with the dynamics. It seems likely that key features of the Kuiper Belt were imprinted at a time when collective effects dominated the transport of energy and angular momentum. Therefore, it is important to heed Ward & Hahn's (1998) warning that published simulations of Kuiper Belt dynamics, by omitting important physics, may be in serious error.

The division of the orbital parameters of the KBOs into three main groups was unexpected and has become the focus of recent theoretical attention. Observed properties worthy of explanation include:

(a) The general absence of KBOs with $a \leq 42$ AU, other than those trapped in mean motion resonances. Long-term numerical integrations show that clearing of the inner belt is a result of strong perturbations by Neptune (Holman & Wisdom 1993, Duncan et al 1995). This is seen in Figure 4, where most nonresonant orbits inside 42 AU have lifetimes $\ll$4 Gyr. Objects originally in this region were quickly scattered away or absorbed by

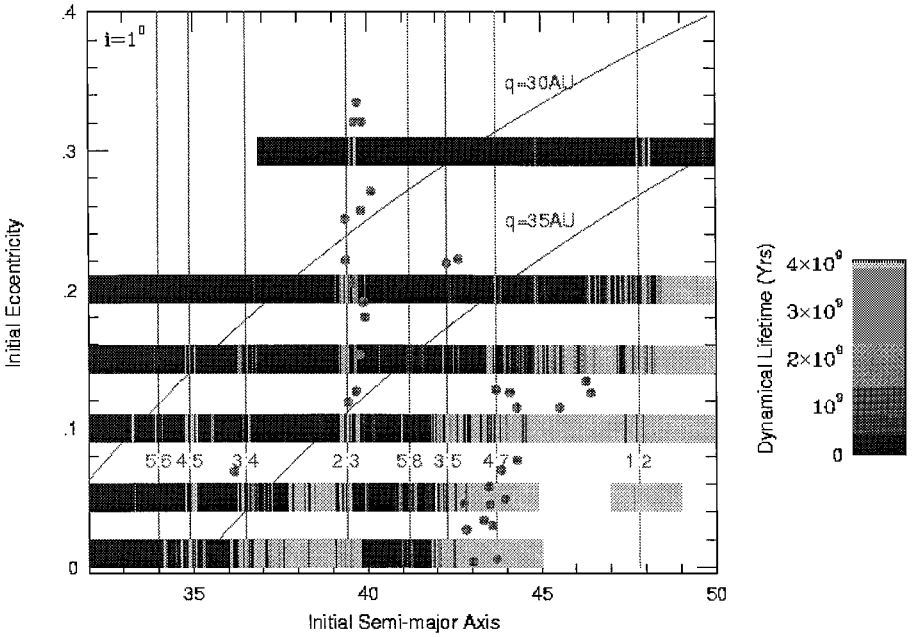

Figure 4 Dynamical simulations of test particle longevity compared with locations of real KBOs (*solid circles: see Figure 2*) in the semi-major axis versus eccentricity plane. Note that the simulations are for assumed inclinations of 1° while the real KBOs exhibit inclinations up to 32° (From Duncan et al 1995).

Neptune. A clear discrepancy exists between numerical simulations and the real Kuiper Belt. Low *e*, low *i* orbits in the 36 to 39 AU range are stable (Figure 4, Duncan et al 1995) and yet no KBOs have been found in this region (Figure 2). Objects in this region might have been removed by resonance sweeping (Malhotra 1995) due to planet migration, or by outward movement of the ν_8 secular resonance due to planet–disk interactions in an early, massive phase. A second empty zone, between 40 and 42 AU, is unstable due to overlapping secular resonances which induce chaotic motion (Knezevic et al 1991, Holman & Wisdom 1993). At greater distances, the influence of Neptune is diminished and nonresonant orbits are stable provided their perihelia remain $\geq$40 AU.

(*b*) The large number of objects trapped in the 3:2 resonance. The numerical integrations of Holman & Wisdom (1993) show that initially circular, coplanar orbits near the 3:2 resonance can develop moderate eccentricities and inclinations simply through the long-term action of planetary perturbations.

This was explored further by Levison & Stern (1995) as a way to explain the orbital properties of Pluto. They found that orbits excited in this way are unstable to unrealistically high libration amplitudes and they suggested that a dissipative process (possibly a collision) might have stabilized Pluto in the 3:2 resonance. Presumably, corresponding collisions would be needed to stabilize the many other Plutinos now known to be in the resonance. However, the distribution of orbital eccentricities predicted by this model is inconsistent with the orbits of Plutinos as determined from recent data (Figure 2). Whereas the majority of their simulated resonant objects have $e < 0.1$, precisely these eccentricities are missing from the observed Plutino population.

A second possible explanation is the resonance-sweeping hypothesis (Malhotra 1995). As originally envisaged, proto-Neptune scattered nearby planetesimals in the surrounding disk, exchanged angular momentum with them and, as a consequence, underwent a radial excursion (Fernandez & Ip 1984). Planetesimals that were scattered inward fell under the control of Uranus, while those scattered outward were either ejected from the planetary system, entered the Oort Cloud, or fell back to the region of the planets to be scattered again. This asymmetry in the fates of scattered objects caused the orbits of Saturn, Uranus and Neptune to expand (Fernandez & Ip 1984) while Jupiter, the innermost massive scatterer, migrated inward to provide the ultimate source of the angular momentum carried away by scattered planetesimals.

As Neptune migrated, its mean motion resonances swept through the planetesimal disk, trapping objects (Figure 5). Malhotra (1995) found that the maximum eccentricity reached by resonantly trapped particles is related to the distance of Neptune's migration. For a first order ($j + 1$:j) resonance (where j is a positive integer),

$$e^2_{final} \approx e^2_{initial} + \left(\frac{1}{j+1}\right) \ln\left(\frac{a_{N,final}}{a_{N,initial}}\right) \tag{3}$$

where $e_{initial}$ and e_{final} are the starting and ending eccentricities of the planetesimal and $a_{N,initial}$, $a_{N,final}$ are the starting and ending semi-major axes of Neptune. For the 3:2 resonance ($j = 2$), with $e_{final} \gg e_{initial}$, the Plutinos (median eccentricity $e_{final} = 0.24$), give $a_{N,initial} \sim 25$ AU, or a total migration of about 5 AU. The 3:2 resonance would have swept from 33 AU to its present location at 39 AU and the more distant 2:1 resonance from 40 AU to its present location at 47.6 AU (Figure 5).

Numerical simulations of the sweeping process give partial agreement with the data (Figure 6). The ranges of eccentricity (and perhaps, inclination) of KBOs trapped in the 3:2 resonance are well matched by the model

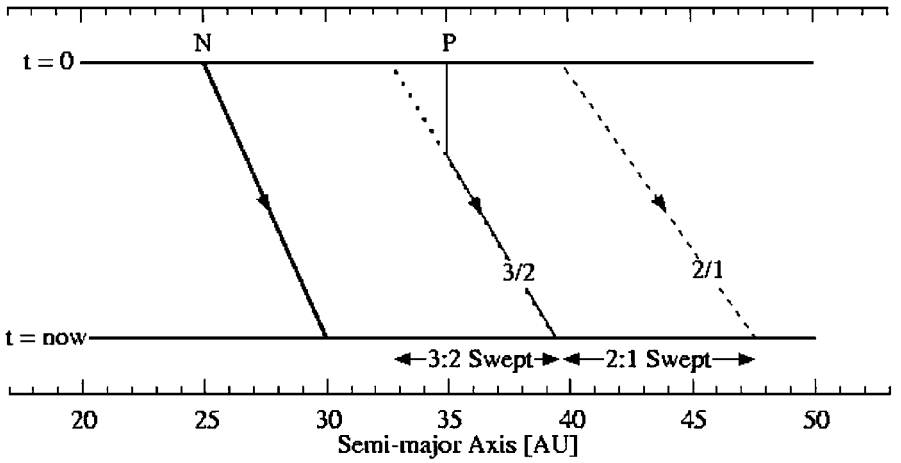

Figure 5 Radial migration of Neptune (*N*) and its 3:2 and 2:1 mean motion resonances. Trapping of Pluto (*P*) into the 3:2 resonance is symbolically illustrated. The zones swept by the 3:2 and 2:1 resonances are marked (Figure slightly modified from Malhotra 1995).

without the need for stabilizing collisions. The high population of 3:2 objects is also faithfully reproduced, because resonance trapping is efficient. Resonance sweeping also explains why apparently stable objects in the 36 to 39 AU region are not found: these bodies would have been swept by the outwardly moving 3:2 resonance. On the other hand, the simulations presented by Malhotra (1995) predict a substantial population of KBOs in the 2:1 resonance, whereas none are seen (Jewitt et al 1998). However, the trapping efficiency is a function of the speed and character of Neptune's migration, of the initial eccentricity and inclination of the planetesimals, and of proto-Neptune's mass (the trapping occurs during the late phases of the growth of the planet). Recently, Ida et al (1998) identified simulations of resonance sweeping in which the 2:1 resonance is left empty. Their simulations differ from Malhotra's in using extremely rapid Neptune migration timescales ($\leq 10^6$ yr) and sub-Neptune masses. This is too fast to be consistent with torques due to planetesimal scattering but might be appropriate for torques exerted by a massive gas disk. The physical significance of this result is not clear. Hydrogen and helium in Neptune (and Uranus) are depleted relative to their solar proportions. This is widely taken as evidence that Neptune grew slowly, reaching its final mass after the escape of the bulk of the gas disk (Lissauer et al 1995, Pollack et al 1996). In this case insufficient mass would be present in the gas disk to accelerate Neptune on 10^6 yr timescales.

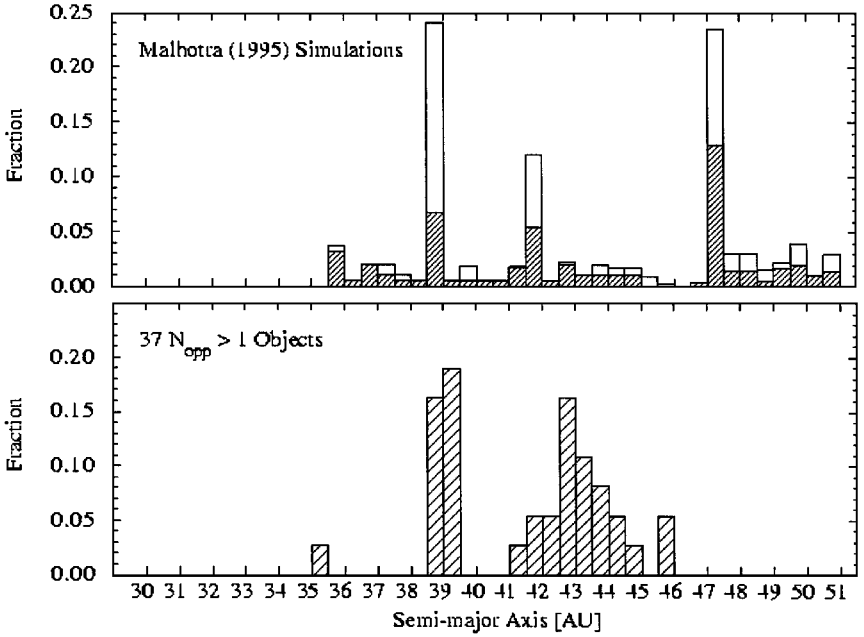

Figure 6 Distribution of semi-major axes of KBOs according to simulations of resonance sweeping due to planetary migration (*top panel*; adapted from Malhotra 1995) compared to the apparent distribution (*bottom panel*). The *shaded histograms* in the top panel indicate results from different sets of initial conditions. A Neptune migration timescale of 2×10^6 yr was adopted.

Whether resonance sweeping is responsible for the Plutinos is unclear. There is little doubt that planetary migration occurred. The gas giant planets must have exchanged angular momentum with the surrounding protoplanetary disk; only the amount and the timescale of the exchange are uncertain.

(*c*) The very wide range of inclinations of both classical and resonant KBOs. As noted, excited inclinations (and eccentricities) are natural consequences of resonance trapping (Holman & Wisdom 1993, Duncan et al 1995, Malhotra 1996). It is more surprising to observe very high inclinations in the classical Kuiper Belt (Figure 3). These inclinations and eccentricities correspond to relative collision velocities near $\Delta V = 1$ km s^{-1}. With a critical specific fragmentation energy near 10^3 J kg^{-1} (Fujiwara et al 1989), the velocity dispersion is large enough to ensure that collisions with objects having only 10^{-3} of the target mass (e.g. a 10 km projectile striking a 100 km target) cause fragmentation. Therefore, impacts in the present day Kuiper Belt are primarily erosive rather than agglomerative, and the KBOs cannot have

grown in the present high-velocity regime (Stern 1996, Farinella & Davis 1996). The inescapable conclusion is that the velocity distribution among the KBOs has been amplified since the epoch of formation. The source of this amplification is a leading puzzle.

The disturbing influence of Neptune is largely restricted to the inner part of the Belt ($a \leq 42$ AU), and cannot explain the high mean e and i of the more distant classical KBOs (e.g. Figures 3 and 4 of Holman & Wisdom 1993 give median $e \sim 0.02$ and $i \sim 1^\circ$ for objects in initially circular, coplanar orbits between $42 \leq R \leq 50$ AU). Mutual gravitational interactions among KBOs may have pumped the velocity dispersion, especially if the early Kuiper Belt were very massive and contained large objects. There is good evidence for the temporary existence of short-lived, Earth-mass objects in the early outer solar system: large-body impacts are thought to account for the basic characteristics of planetary spin (Dones & Tremaine 1993) including the large obliquity of Uranus (Slattery et al 1992). Morbidelli & Valsecchi (1997) found that a handful of Earth-sized projectiles could excite the velocity dispersion of the KBOs and lead to extensive depopulation. In their model, the degree of damage inflicted on the Kuiper Belt is a sensitive function of the assumed masses and trajectories of the scattered objects. While the choice of these parameters is necessarily arbitrary, it appears that a few well-aimed Earth-mass bodies can disrupt the Belt and leave a dynamically excited remnant with traits similar to those observed (Petit et al 1998). It is not clear how to reconcile the massive-planetesimals hypothesis with the resonance-sweeping hypothesis for the population of the mean motion resonances. Massive scatterers capable of stirring up the velocity dispersion to 1 km s^{-1} would also dislodge most objects from resonance with Neptune. To argue that resonance sweeping occurred after the epoch of the massive scatterers is also problematic because the efficiency of trapping into resonance decreases as the initial eccentricity and inclination increase (Malhotra 1995): capture from nearly circular ecliptic orbits is much preferred. This dilemma currently evades resolution.

(*d*) The source of the short-period comets. The short-period comets have dynamical lifetimes of order 10^5 to 10^6 yr (Levison & Duncan 1994) and must be continually replenished if they are to maintain a steady-state population over the age of the solar system. There is a consensus that the Kuiper Belt is the source of the short-period comets, but the precise location of the source remains unidentified. Chaotic zones at the edges of resonances represent one plausible source (Morbidelli 1997). The chaotic zones may be populated and depopulated by mutual scattering as well as by dynamical chaos (Ip & Fernandez 1997). Randomly deflected scattered KBOs may also

contribute to the short-period comet supply (Duncan & Levison 1997), as might the semi-stable 1:1 Lagrangian resonances with the major planets and the narrow, stable ring at 26 AU identified by Holman (1997). Potentially, all of these sources contribute to the flux of short-period comets.

CUMULATIVE LUMINOSITY FUNCTION, SIZE DISTRIBUTION

The cumulative luminosity function (CLF) is the number of KBOs per unit area of sky brighter than a given limiting magnitude, measured as a function of the magnitude. The CLF provides a measure of the size distribution and total number of KBOs and is therefore a quantity of particular observational interest. The CLF is well defined in the magnitude 20 to 26 range (Figure 7). At brighter magnitudes, the available constraints are based mainly on photographic data, and are difficult to calibrate and interpret. At fainter magnitudes, a measurement using the Hubble Space Telescope (Cochran et al 1995) has proved controversial. Brown, Kulkarni and Liggett (1997) found that the reported number of KBOs is, implausibly, two orders of magnitude beneath the sensitivity limits of the HST, a result that Cochran et al (1998) dispute. Independent confirmation of the measurement is desirable.

The CLF is described by

$$\log[\Sigma(m_R)] = \alpha(m_R - m_0) \tag{4}$$

where $\Sigma(m_R)$ is the number of objects per square degree brighter than red magnitude m_R, and α and m_0 are constants. Least squares fits to the CLF give $\alpha = 0.58 \pm 0.05$, $m_0 = 23.27 \pm 0.11$ ($20 \leq m_R \leq 25$; Jewitt et al 1998) and $\alpha = 0.54 \pm 0.04$, $m_0 = 23.20 \pm 0.10$ ($20 \leq m_R \leq 26.6$; Luu and Jewitt 1998b). Gladman et al (1998) used a different subset of the data (including some of the photographic constraints and the uncertain HST measurement) and a different (maximum likelihood) fitting method to find $\alpha = 0.76^{+0.10}/_{-0.11}$, $m_0 = 23.40^{+0.20}/_{-0.18}$ ($20 \leq m_R \leq 26$). Within the uncertainties, the various fits are consistent. In fact, the true uncertainties are likely to be larger than indicated because of hitherto ignored systematic errors. For example, it is probable that the surface density is a function of ecliptic longitude, owing to the nature of the Neptune-avoiding resonant objects, and yet no allowance for longitudinal effects has been attempted by the observers.

The gradient of the CLF is determined by the size and spatial distributions of the KBOs, and by the distribution of albedo among these objects. Simple models in which the size distribution is taken to be a power law with index $-\beta$, the spatial distribution is another power law with index -2, and the albedo is constant give $\beta \approx 4.0 \pm 0.5$ (Jewitt et al 1998, Luu & Jewitt 1998b) to $\beta \approx 4.8$

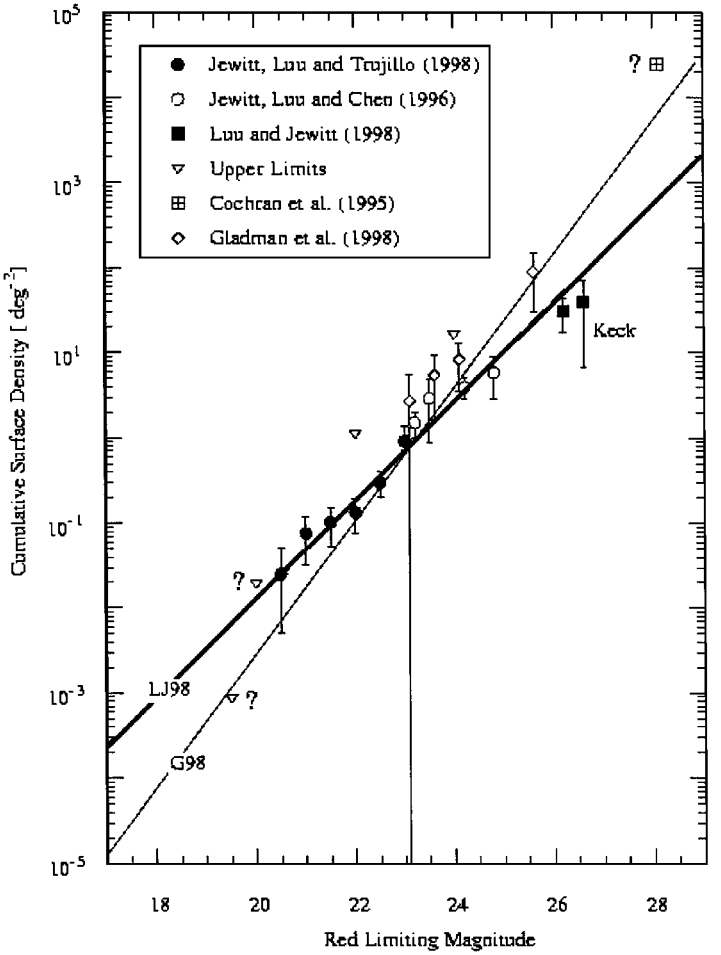

Figure 7 Cumulative luminosity function (CLF) of the Kuiper Belt. Lines through the data mark fits by Luu and Jewitt 1998b (*thick line*) and Gladman et al 1998 (*thin line*).

(Gladman et al 1998). Also, the albedo might be a systematic function of object size (gravity), adding another unmodeled effect to the CLF. In any event, the size distribution of KBOs (diameter greater than or approximately equal to 100 km) is probably steeper than the canonical $\beta = 3.5$ as produced by shattering collisions (Dohnanyi 1969).

It is not yet known whether the size distributions of the different dynamical classes in the Kuiper Belt are the same, but it is easy to think of reasons why

they should not be. For example, impulses larger than a few tens of m s^{-1} (from collisions and mutual gravitational scattering) are capable of dislodging objects from resonance. Because small KBOs suffer larger average collisional impulse velocities than their massive counterparts, resonant objects may have a steeper size distribution than the classical Belt.

The total numbers of KBOs must be estimated by extrapolation from surveys of limited areas of the ecliptic. The extrapolations hinge on knowledge of the spatial extent of the Kuiper Belt, both radially and perpendicular to the ecliptic. Regions beyond $R \sim 50$ AU are poorly sampled by the available data, so that the number of objects is known only in the range $30 \leq R \leq 50$ AU. Furthermore, highly inclined KBOs spend a smaller fraction of each orbit near the ecliptic than KBOs of small inclination, and are thus subject to an observational bias. For this reason, the data provide only a lower limit to the intrinsic thickness of the Belt. The apparent thickness is $10^\circ \pm 1$ FWHM (Jewitt et al 1996) but, corrected for bias, the intrinsic thickness may be 30° or more, with no statistically significant difference between the classical and resonant populations.

The number of KBOs larger than 100 km in diameter (assuming 0.04 geometric albedo) in the 30 to 50 AU distance range is $\sim 10^5$ (Jewitt et al 1998). By extrapolation, assuming size index $\beta = 4$, the number of KBOs larger than 5 km diameter in the 30 to 50 AU region is 8×10^8, but with an uncertainty approaching an order of magnitude. Meaningful comparison with the number of comets required to replenish the short-period population for the age of the solar system is difficult because the sizes of the comets are not well known. The numbers seem of the right order, however (Duncan et al 1988, Duncan et al 1995). The total mass in observable (diameter $\geq$100 km) objects is of order $0.1 M_{Earth}$ ($1 M_{Earth} = 6 \times 10^{24}$ kg; Jewitt et al 1996, Jewitt et al 1998, Luu & Jewitt 1998), based on an assumed bulk density 1000 kg m^{-3} and a power law differential size distribution with index $q = 4$. The mass is uncertain primarily because the KBO diameters are computed on the untested assumption of dark surfaces (albedo 0.04). The derived mass is consistent with the dynamical limit to the mass, $\sim 1 M_{Earth}$ (Hamid et al 1969).

PHYSICAL OBSERVATIONS

Optical (Luu & Jewitt 1996, Green et al 1997) and near-infrared colors (Jewitt & Luu 1998) of KBOs exhibit a diversity that suggests a range of surface types among KBOs. The best spectral discriminant is the V-J color index, which measures the ratio of the surface reflectances at V (approximately 0.55 μm) and J (approximately 1.2 μm) wavelengths. Figure 8 shows that V-J varies from 0.7 (1996 TO66) to 2.2 (1996 TP66) in the Kuiper Belt (and up to 2.6 in the Centaur 5145 Pholus). V-J can be measured to a 1σ accuracy of about

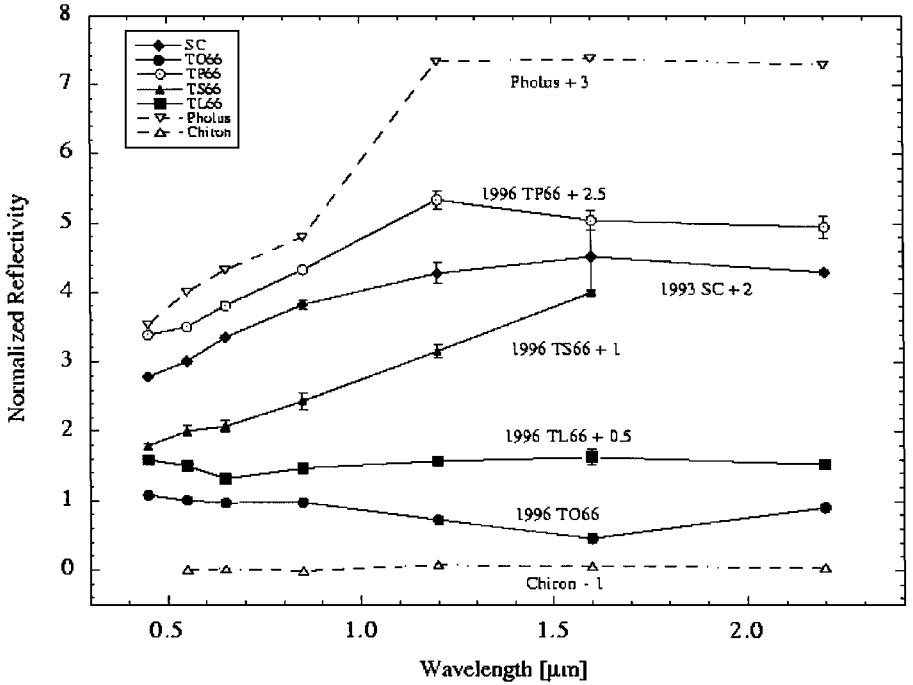

Figure 8 Normalized reflectivity versus wavelength for five KBOs. The KBOs are vertically offset for clarity, but preserve a fixed scale. Reflectivities of Centaur objects 2060 Chiron and 5145 Pholus are shown for comparison. (From Jewitt & Luu 1998).

0.1 mag., so that the color differences are highly significant ($\sim 20\sigma$). Tegler & Romanishin (1998) further claim that the KBOs are divided by optical color into two distinct classes with no intermediate examples, but the color separation of the groups exceeds the formal uncertainty of measurement by only a few times the 1σ accuracy of the colors. This intriguing result awaits independent confirmation.

Bombardment of simple ice mixtures (H_2O, CO_2, CO, NH3) by energetic particles (photons or atomic nuclei) is known to cause surface darkening and modification of the chemical structure of the surface to a column density of ~ 100 g cm^{-2} (Johnson et al 1987, Moroz et al 1998). Incident particle energy is dissipated by breaking chemical bonds which then recombine to make new, structurally complex compounds. Hydrogen atoms liberated in this process are sufficiently small that they can escape from the irradiated material even at the low temperatures prevailing in the Kuiper Belt (~ 50 K). The resulting "radiation mantle" is a hydrogen-poor, carbon-rich (and therefore dark),

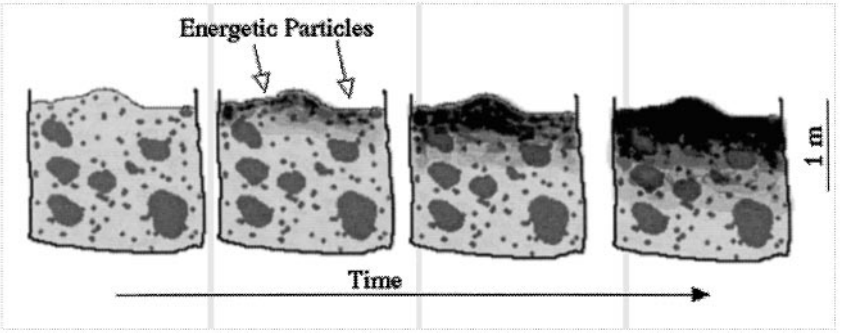

Figure 9 Development of an irradiation mantle. A KBO consisting of a mixture of refractory particles and common ices is bombarded by high-energy cosmic rays. Over time, a hydrogen-depleted crust of high molecular weight and of column density $\sim$100 g cm^{-2} develops. Carbon compounds in the mantle are responsible for the low albedo.

high-molecular-weight compound having low volatility (Figure 9). The timescale for saturation damage of the surface layer by cosmic rays is of order $10^{8\pm1}$ yrs (Shul'man 1972), but measurable surface darkening may occur much more rapidly. The surfaces of cometary nuclei are believed to be coated by such material, and it is natural to expect the same of KBOs. Within this context, it is difficult to see why the KBOs would vary in optical color from neutral to very red, or why the V-J index should be so variable from object to object.

A consensus regarding the origin of spectral diversity has yet to emerge. One possibility is that KBOs are occasionally resurfaced by collisionally generated debris (Luu & Jewitt 1996). The surface color would change because material excavated from depths greater than a few meters is unaffected by cosmic-ray irradiation. The instantaneous surface color would be determined primarily by the time since resurfacing. This remains a plausible hypothesis for color diversity only so long as the timescales for irradiation and resurfacing are of the same order. Unfortunately, neither timescale is well known. Should the color distributions really be bimodal, the resurfacing hypothesis would be immediately ruled out because partial resurfacing always produces intermediate colors.

A second possibility is that different KBOs have intrinsically different surface compositions, either because they formed differently, or because of long-term evolutionary effects. For example, large KBOs might be more thoroughly outgassed than small KBOs as a result of greater radioactive heating, and would be better at retaining surface frost deposits. However, at present, there is no compelling evidence for a color-size relation among the KBOs.

Energetic irradiation should produce a spectrally bland material corresponding to the destruction of all hydrogen bonds and the loss of hydrogen to space.

Spectral evidence is limited to near infrared spectra of KBOs 1993 SC and 1996 TL66. The heavily smoothed spectrum of 1993 SC is reported to show absorption bands reminiscent of (but not specifically identified with) complex hydrocarbon compounds (Brown et al 1997). The spectrum of 1996 TL66 is featureless and flat (Luu & Jewitt 1998). More spectra are urgently needed.

The albedos of KBOs have yet to be measured. The standard technique applied to main-belt asteroids is the simultaneous measurement of optical (reflected sunlight) and thermal (absorbed and re-radiated sunlight) radiation, from which both the cross section and the albedo can be measured. The Planck maximum for objects at 40 AU (temperature $\sim$50 K) falls near 60 μm wavelength, which is inaccessible from the ground. Measurements using the ISO orbiting telescope yielded marginal detections of 1993SC and 1996TL66, from which low (few percent) albedos may be inferred (Nick Thomas, private communication). Stellar occultations may soon be available from the TAOS project and others (Brown & Webster 1997), from which diameters and albedos might be directly inferred. At the present, however, all KBO diameters are computed on the assumption of a uniform red albedo $p_R = 0.04$. This value is adopted from measurements of the albedos of cometary nuclei and Centaurs (bodies in transition from the Kuiper Belt to the short-period comets), most of which tend to be very dark. For example, if the albedo should be higher by a factor of 10, the derived KBO diameters would decrease by a factor $10^{1/2}$, and the masses by a factor $10^{3/2}$. The diversity of surface types indicated by Figure 8, for example, certainly suggests that the albedos of KBOs may not all be the same. There is some evidence that the albedo is a function of object diameter (Figure 10). The largest objects have sufficient gravitational attraction to retain weak atmospheres from which albedo-enhancing surface frosts may be deposited. Conclusions about sizes and masses of KBOs are thus rendered uncertain.

DUST

Collisions between KBOs and the impacts of interstellar grains should provide a continuous source of dust. Liou et al (1996) presented numerical integrations of the equation of motion for dust particles released in the Kuiper Belt. They included radiation pressure, plasma drag, and Poynting-Robertson drag forces, as well as gravitational forces due to the planets (except Mercury and Pluto). Kuiper Belt dust particles that survive to cross the orbit of Earth do so with small eccentricities and inclinations, and would be difficult to distinguish from asteroidal dust grains on the basis of their orbital parameters alone. Liou, Zook, and Dermott found that $\sim$20 percent of the modeled 1-to-9-μm–diameter particles survive to reach the sun (the majority are ejected from the solar system

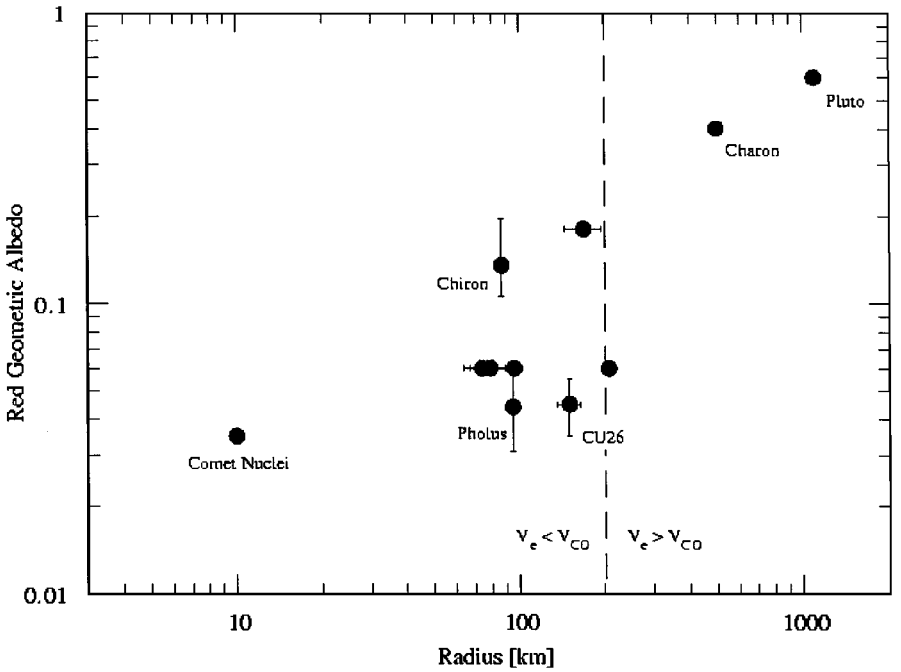

Figure 10 Red geometric albedo versus radius for a variety of outer solar system objects. *Dashed vertical line* marks $V_e = V_{CO}$, where V_e is the escape velocity (at assumed density $\rho = 1000$ kg m^{-3}) and V_{CO} is the thermal velocity of a CO molecule at $T = 40$ K. There is a trend for albedo to increase with object size. However, this trend is dominated by Pluto and Charon, objects both large enough to retain weak atmospheres.

by the gas giant planets). However, timescales for the collisional destruction of Kuiper Belt grains by interstellar dust particles (Figure 11) are less than the dynamical transport times (which cluster near 10^7 yr) for many of the small particles modeled by Liou et al (1996). Therefore, the survival probability of Kuiper Belt dust entering the inner solar system must be considerably smaller than 20 percent, and the size distribution of the surviving grains will be modified by shattering collisions with interstellar grains. Such particles might one day be identified in terrestrial stratospheric collections (Brownlee 1985) by their high solar wind track densities (due to long transport times from the Kuiper Belt).

I bracket the current dust production rate in the belt as follows. A lower limit is given by the rate of erosion due to interstellar dust impacts, $dM_d/dt \geq 4 \times 10^2$ kg s^{-1} (Yamamoto & Mukai 1998). An upper limit may be estimated by dividing the Kuiper Belt mass (approximately $0.1 M_{Earth}$; Jewitt et al 1998) by

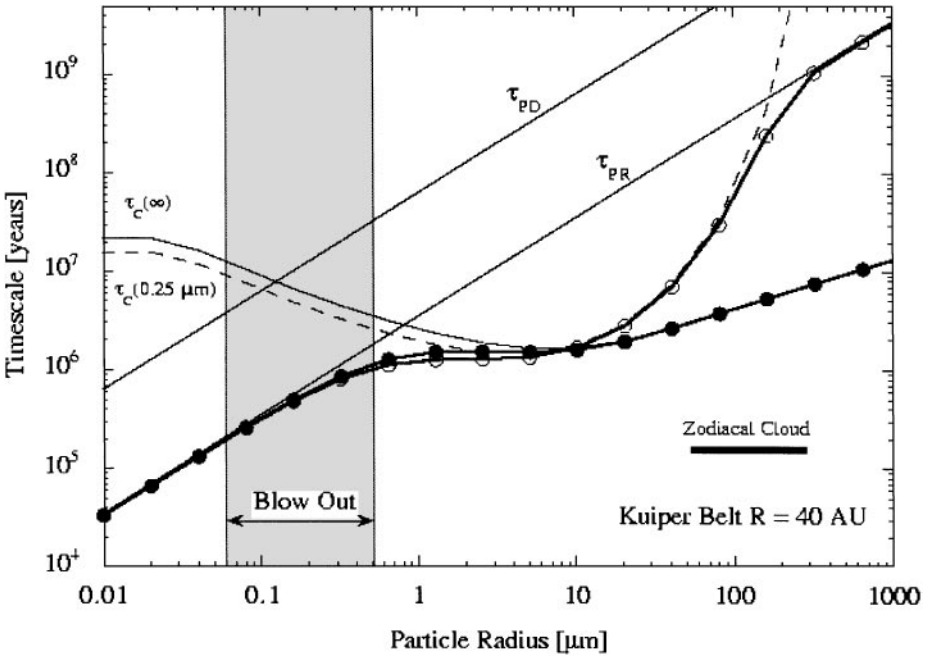

Figure 11 Timescales for Poynting-Robertson decay (τ_{pr}), plasma drag (τ_{pd}) and collision with interstellar dust (τ_c) all plotted as a function of radius for particles at 40 AU in the Kuiper Belt. *Shaded region* marks particles likely to be ejected from the solar system by radiation pressure. *Lines with circles* show the lifetimes to all three processes combined: *line with filled circles* corresponds to $a_0 = \infty$, and that with empty circles $a_0 = 0.25\ \mu$m. The interstellar dust particles were assumed to follow a power law size distribution with differential index -3.5, and with maximum particle radius a_0 (From Jewitt & Luu 1997).

the age of the solar system (4.6 Gyr), giving $dM_d/dt \leq 10^7$ kg s^{-1}. Thus:

$$4 \times 10^2 \text{ kg s}^{-1} \leq dM_d/dt \leq 10^7 \text{ kg s}^{-1} \tag{5}$$

is given for the current rate of dust production. For comparison, the production rate needed to sustain the Zodiacal Cloud is $\sim 10^4$ kg s^{-1} (Leinert et al 1983, Grün et al 1994).

With both foreground (Zodiacal Cloud) and background (galactic) confusion, it is perhaps not surprising that attempts to measure thermal emission from Kuiper Belt dust have failed (Backman et al 1995). However, there is one reported in situ detection of dust in the Kuiper Belt: Gurnett et al (1997) counted dust impacts using plasma wave analyzers on the Voyager 1 and 2 spacecraft. They determined an average number density of micron-sized grains

$N_1 = 2 \times 10^{-8}$ m^{-3} along the two Voyager trajectories, beyond 30 AU. The plasma wave analyzers are sensitive to only a narrow range of particle sizes: impacts below the threshold mass 1.2×10^{-14} kg (corresponding to particle radius 1.4 μm at unit density) do not excite measurable plasma waves (Gurnett et al 1997) while larger impacts are, presumably, rare. The average mass of a grain is taken as $m_d \sim 2 \times 10^{-14}$ kg (c.f. Gurnett et al 1997) and the volume of the Kuiper Belt (represented as an annular slab with inner and outer radii 30 AU and 50 AU, respectively, and a thickness of 10 AU) as $V \sim 2 \times 10^{38}$ m^3. The total mass of dust in micron-sized particles is then $M \sim m_d N_1 V \sim 8 \times 10^{16}$ kg. With a $\tau_c \sim 10^6$ yr dust lifetime, the implied production rate in micron-sized particles is of order $M/\tau_c \sim 3 \times 10^3$ kg s^{-1}, which is near the lower limit in Equation 5.

If the dust size distribution extends far above the micron size range, the Voyager impact measurements provide only a lower limit to the total rate of production of debris. In a Dohnanyi (1969) type power law distribution with index -3.5, micron-sized particles contain only $\sim$1/16th of the mass, when measured to maximum radius 1 mm ($\sim$1/500th when measured to 1 m). The nondetection of centimeter-sized particles from Pioneer 10 (Anderson et al 1998) unfortunately does not provide a strong constraint on the dust size distribution.

CONSTRAINTS ON THE ORIGIN OF THE KUIPER BELT

Factors relating to the origin and evolution of the Kuiper Belt may be summarized in this manner:

(*a*) The surface density of the condensible part of the planetary mass obtained by smearing the masses of the giant planets is given roughly by $\sigma(R) \approx 10(10/R)^{3/2}$ [kg m^{-2}], where R is heliocentric distance measured in AU (Weidenschilling 1977, c.f. Pollack et al 1996). The mass obtained by integrating this surface density over the $30 \leq R \leq 50$ AU annulus is $\sim 25 M_{Earth}$, or about 10^2 times the estimated mass of the present Kuiper Belt. Either the extrapolation of $\sigma(R)$ beyond Neptune is invalid (i.e., the protoplanetary disk had an edge) or a large part of the mass initially present in the $30 \leq R \leq 50$ AU zone has been removed.

(*b*) Given only the present mass in the 30-to-50 AU region, the timescales for growth of the KBOs by binary accretion to 100 km and 1000 km scales are much longer than the age of the solar system (Stern 1995, Kenyon & Luu 1998). Such growth is therefore impossible, with the implication that

either the KBOs formed elsewhere and were transported to their present locations by processes unknown or that the Kuiper Belt surface density was originally larger than it is at present.

(*c*) Perturbations from Neptune exert a major disturbing influence on the adjacent Kuiper Belt (Holman & Wisdom 1993, Levison & Duncan 1993, Duncan et al 1995), raising the velocity dispersion and decreasing the accretion rate. Therefore it is probable that the KBOs (in the inner part of the belt) were formed before Neptune (Stern 1996). However, assuming $35M_{Earth}$ between 35 and 50 AU, Stern (1996) obtained Pluto growth times near 10^9 yr, which is longer than the 10^8 yr timescale for formation of Neptune (Lissauer et al 1995, Pollack et al 1996). Only recently have more compatible Pluto growth times have been obtained. Kenyon & Luu (1998) assert that the 10^9 yr timescales obtained by Stern were due to a binning error in the solution of the coagulation equation. Their numerical experiments show that 1000 km sized objects could form in $<10^8$ yr provided the initial Kuiper Belt mass is 10–$30M_{Earth}$ (Kenyon & Luu 1998). Again, the implication is that a substantial mass of material has been lost from the Kuiper Belt.

Several possibilities have been suggested to explain the depletion of mass from the Kuiper Belt. Long-term numerical integrations (e.g. Holman & Wisdom 1993; Duncan et al 1995) show that the decline in the number of KBOs is approximately logarithmic with time and therefore too slow to be the main cause of the depletion. The resonance-sweeping mechanism also appears incapable of losing 99 percent of the mass. Numerical experiments show that more than 50 percent of initially nonresonant objects are captured into mean motion resonances (Malhotra 1995). Admittedly, these experiments are simplistic, and the capture probability has not been assessed over a full range of initial orbital eccentricities. As noted by Fernandez & Ip (1984) and Malhotra (1995), the motion of Neptune is taken to be smooth and continuous. In reality, scattering of massive planetesimals would lend a stochastic character to Neptune's radial excursion, resulting in a decreased trapping efficiency. Stern & Colwell (1997) suggest that collisional grinding could have eroded the 30 AU–50 AU region from 10 to $35M_{Earth}$ down to the observed $\sim 0.1M_{Earth}$ in 10^9 yr. However, their model neglects velocity evolution and dynamics and is therefore of uncertain significance. Crucially, they note that sufficient erosion is obtained only if the mean eccentricity is somehow sustained above $e \geq 0.1$. In any case, the larger KBOs (namely, those detected in current ground-based surveys) cannot be destroyed by collisional grinding (Farinella & Davis 1996). For collisions to have removed 99 percent of the initial mass, one would have

to postulate a steep initial size distribution ($q \sim 5$) in which objects large enough to escape comminution carry only one percent of the mass.

(*d*) The existence of the Pluto-Charon binary sets additional constraints on the Kuiper Belt. First, it is widely supposed (based on the large specific angular momentum of the planet-satellite pair) that Charon was formed by a giant impact into Pluto (McKinnon 1989, Dobrovolskis et al 1997). If so, this impact must have occurred prior to the capture of Pluto into the 3:2 resonance, for otherwise the recoil would have knocked the planet out of resonance (Hahn & Ward 1995). Second, the rate of impacts into Pluto large enough to eject Charon is presently vanishingly small. Accordingly, the existence of an impact-formed Charon suggests a much–higher-density Kuiper Belt, perhaps containing many Pluto-sized bodies (Stern 1991). Third, the eccentricity of the orbit of Charon should be tidally damped to a very low level ($e \ll 10^{-3}$) on timescales that are short compared to the age of the solar system. Surprisingly, Tholen & Buie (1997) have measured $e = (7.6 \pm 0.5) \times 10^{-3}$. If confirmed, this eccentricity will set important constraints on the impact rate in the modern-day Kuiper Belt.

SUMMARY

About 10^5 objects with diameters in excess of 100 km orbit the sun between 30 AU (the orbit of Neptune) and 50 AU (the practical limit of existing surveys). These objects obey a differential power law size distribution with index $q \sim -4$. The distribution seems to extend smoothly to Pluto (diameter ~2300 km) and allows the possibility that other Pluto-sized objects await discovery. The combined mass of these objects is about $0.1 M_{Earth}$. When extrapolated to small sizes, the $q = -4$ distribution predicts that the total number of trans-Neptunian objects larger than 1 km diameter is 10^{11}. However, the size distribution of bodies smaller than 100 km in diameter is obtained by extrapolation and has not been confirmed by direct observation.

The orbits of the KBOs are divided into three main groups. So-called classical KBOs orbit the sun with semi-major axes $42 \leq a \leq 50$ AU, possess small eccentricities and maintain a large separation from Neptune even at perihelion. Their orbits appear stable on timescales longer than the age of the solar system. About two thirds of the KBOs belong to the classical group. Most of the remaining objects reside in mean motion resonances with Neptune. The 3:2 resonance at $a = 39.4$ AU is particularly densely populated. Pluto is the largest of the tens of thousands of objects trapped in this resonance. The scattered KBOs follow large, eccentric orbits with perihelia near 35 AU, close enough to Neptune to permit weak dynamical control by that planet on billion year timescales. One

example, 1996 TL66, is presently known. The inferred population is large, and may even dominate the total mass of trans-Neptunian objects.

The abundance of resonant objects (about 35 percent in the raw data and about 10 to 15 percent when corrected for the effects of observational bias) may provide important clues about the formation and early evolution of the Kuiper Belt. The resonance-sweeping hypothesis (in which Neptune's orbit expanded during planet growth) makes verifiable predictions of the inclination and eccentricity distributions and of the resonance population ratios. In its present guise, this hypothesis suggests a total Neptune excursion from 25 AU to the present 30 AU, on a timescale that was evidently short.

The velocity dispersion among KBOs is near 1 km s^{-1}, suggesting that collisions are largely erosive and that the velocity dispersion has been amplified since the formation epoch. Excitation of the orbits of the resonant KBOs is an expected consequence of trapping into the resonance. However, the nonresonant orbits of classical KBOs are equally excited, suggesting the action of a more general disturbing agent. One suggested possibility is that massive scattered objects were projected through the Kuiper Belt during the late stages of Neptune accretion, stirring up the velocity distribution of the KBOs as they repeatedly passed through.

The combined mass of KBOs in the 30 to 50 AU region is too small for these objects to have grown by accretion in the 10^8 yrs prior to the emergence of Neptune. Roughly $10 M_{Earth}$ of material are needed to ensure growth of Pluto-sized objects on this timescale. By implication, the present Kuiper Belt is a mere shadow of its former self, with about 99 percent of the initial mass now lost. The loss mechanism remains unidentified.

In short, our understanding of the formation and evolution of the Kuiper Belt is currently incomplete, even confused. This is to be expected in a field that is still very young. As more and better observations of KBOs are obtained, existing models will become more tightly constrained and new and unexpected ones will suggest themselves.

ACKNOWLEDGMENTS

I thank the National Aeronautics and Space Administration for support.

NOTE ADDED IN PROOF

Subsequent to the completion of this review two KBOs were identified as possible residents of the 2:1 mean motion resonance. 1996 TR66 has semimajor axis $a \sim 48.2$ AU, eccentricity $e \sim 0.40$ and inclination $i \sim 12$ degree, while the corresponding quantities for 1997 SZ10 are $a,e,i = 48.3$ AU, 0.37, 12 degree (Brian Marsden, IAU Circular 7073, December 26, 1998). When combined with the factor $\sim$3 observational bias against detecting the more distant 2:1

objects (Jewitt, et al 1998), the data are statistically consistent with the hypothesis that the populations in the 3:2 and 2:1 resonances are of the same order. This, in turn, is compatible with a basic prediction of the resonance-sweeping hypothesis as presented by Renu Malhotra (1995).

Literature Cited

Anderson J, Lau E, Scherer K, Rosenbaum D, Teplitz V. 1998. Kuiper belt constraint from Pioneer 10. *Icarus* 131:167–70

Backman DE, Dasgupta A, Stencel RE. 1995. Model of a Kuiper belt small grain population and resulting far-IR emission. *Ap. J. Lett.* 450:35–38

Baum WA, Martin LJ. 1985. Testing the comet belt hypothesis. *Publ. Astron. Soc. Pac.* 97:892

Brown ME, Kulkarni SR, Liggett TJ. 1997. An analysis of the statistics of the Hubble Space Telescope Kuiper belt object search. *Ap. J. Lett.* 490:119–22

Brown MJ, Webster RL. 1997. Occultations by Kuiper belt objects. *MNRAS* 289:783–86

Brown R, Cruikshank D, Pendleton Y, Veeder G. 1997. Surface composition of Kuiper belt object 1993 SC. *Science* 276:937–39

Brownlee D. 1995. Cosmic dust: collection and research. *Annu. Rev. Earth Planet Sci.* 13:147–73

Cochran AL, Cochran WD, Torbett MV. 1991. A deep imaging search for the Kuiper disk of comets. *Bull. Am. Astron. Soc.* 23:131

Cochran AL, Levison HF, Stern SA, Duncan MJ. 1995. The discovery of Halley-sized Kuiper belt objects. *Ap. J.* 455:342–46

Cochran AL, Levison HF, Tamblyn P, Stern SA, Duncan MJ. 1998. Calibration of the HST Kuiper belt object search; setting the record straight. *Ap. J.* 503:L89–93

Dobrovolskis A, Peale S, Harris A. 1997. Dynamics of the Pluto-Charon binary. In *Pluto and Charon*, ed. A Stern, D Tholen, pp. 159–90. Tucson: Univ. Ariz. Press

Dohnanyi J. 1969. Collisional models of asteroids and their debris. *J. Geophys. Res.* 74:2531–54

Dones L, Tremaine S. 1993. On the origin of planetary spins. *Icarus* 103:67–92

Duncan M, Levison H. 1998. A disk of scattered icy objects and the origin of Jupiter-family comets. *Science* 276:1670–72

Duncan M, Levison H, Budd S. 1995. The dynamical structure of the Kuiper belt. *Astron. J.* 110:3073–81

Duncan M, Quinn T, Tremaine S. 1988. The origin of short-period comets. *Ap. J.* 328:69–73

Edgeworth KE. 1943. The evolution of our planetary system. *J. Br. Astron. Soc.* 53:181–88

Edgeworth KE. 1949. The origin and evolution of the solar system. *MNRAS* 109:600–9

Farinella P, Davis D. 1996. Short-period comets: primordial bodies or collisional fragments? *Science* 273:938–41

Fernandez J. 1980. On the existence of a comet belt beyond Neptune. *MNRAS* 192:481–91

Fernandez J, Ip W-H. 1983. On the time evolution of the cometary influx. *Icarus* 54:377–87

Fernandez J, Ip W-H. 1984. Some dynamical aspects of the accretion of Uranus and Neptune. *Icarus* 58:109–20

Fujiwara A, Cerroni P, Davis D, Ryan E, di Martino M, et al. 1989. Experiments and scaling laws for catastrophic collisions. In *Asteroids II*, ed. RP Binzel, T Gehrels, MS Matthews, pp. 240–65. Tucson: Univ. Ariz. Press

Gladman B, Kavelaars J, Nicholson P, Loredo J, Burns J. 1989. Pencil-beam surveys for faint trans-Neptunian objects. *Astron. J.* 116:2042–54

Green SF, McBride N, O'Ceallaigh DP, Fitzsimmons A, Williams IP, Irwin MJ. 1997. Surface reflectance properties of distant solar system bodies. *MNRAS* 290:86–92

Grun E, Gustafson E, Mann I, Baguhl M, Morfill GE, et al. 1994. Interstellar dust in the heliosphere. *Astron. Ap.* 286:915–24

Gurnett DA, Ansher JA, Kurth WS, Granroth LJ. 1997. Micron-sized dust particles detected in the outer solar system by the Voyager 1 and 2 plasma wave instruments. *Geophys. Res. Lett.* 24:3125–28

Hahn J, Ward W. 1995. Resonance passage via collisions. *Lunar Planet. Sci.* 26:541–42

Holman M. 1997. A possible long-lived belt of objects between Uranus and Neptune. *Nature* 387:785–88

Holman M, Wisdom J. 1993. Dynamical stability in the outer solar system and the delivery of short period comets. *Astron. J.* 105:1987–99

Ida S, Tanaka H, Bryden G, Lin D. 1998. Migra-

tion of proto-Neptune and the orbital distribution of trans-Neptunian objects. Preprint: U.C. Santa Barbara Press
Ip W-H, Fernandez J. 1997. On dynamical scattering of Kuiper belt objects in 2:3 resonance with Neptune into short-period comets. *Astron. Ap.* 324:778–84
Jewitt D, Luu J. 1993. Discovery of the candidate Kuiper belt object 1992 QB1. *Nature* 362:730–32
Jewitt D, Luu J, Chen J. 1996. The Mauna Kea-Cerro Tololo (MKCT) Kuiper belt and Centaur survey. *Astron. J.* 112:1225–38
Jewitt D, Luu J, Trujillo C. 1998. Large Kuiper belt objects: the Mauna Kea 8k CCD survey. *Astron. J.* 115:2125–35
Jewitt DC, Luu JX. 1995. The solar system beyond Neptune. *Astron. J.* 109:1867–76
Jewitt DC, Luu JX. 1997. The Kuiper belt. In *From Stardust to Planetesimals. ASP. Conf. Ser., 122*, ed. YJ Pendleton, A Tielens, p. 335–45
Jewitt DC, Luu JX. 1998. Optical-infrared spectral diversity in the Kuiper belt. *Astron. J.* 115:1667–70
Johnson RE, Cooper JF, Lanzerotti LJ, Strazzulla G. 1987. Radiation formation of a nonvolatile comet crust. *Astron. Ap.* 187:889–92
Kenyon SJ, Luu JX. 1998. Accretion in the early Kuiper belt. I. coagulation and velocity evolution. *Astron. J.* 115:2136–60
Knezevic Z, Milani A, Farinella P, Froeschle Ch, Froeschle Cl. 1991. Secular resonances from 2 to 50 AU. *Icarus* 93:316–30
Kowal C. 1989. A solar system survey. *Icarus* 77:118–23
Kuiper GP. 1951. On the origin of the solar system. In *Astrophysics*, ed. JA Hynek, pp. 357–424. New York: McGraw-Hill
Leinert C, Roser S, Buitrago J. 1983. How to maintain the spatial distribution of interplanetary dust. *Astron. Ap.* 118:345–57
Levison HF, Duncan MJ. 1990. A search for proto-comets in the outer regions of the solar system. *Astron. J.* 100:1669–75
Levison HF, Duncan MJ. 1993. The gravitational sculpting of the Kuiper belt. *Ap. J. Lett.* 406:35–38
Levison HF, Duncan MJ. 1994. The long-term dynamical behavior of short-period comets. *Icarus* 108:18–36
Levison HF, Stern SA. 1995. Possible origin and early dynamical evolution of the Pluto-Charon binary. *Icarus* 116:315–39
Liou J-C, Zook HA, Dermott SF. 1996. Kuiper belt dust grains as a source of interplanetary dust particles. *Icarus* 124:429–40
Lissauer J, Pollack J, Wetherill G, Stevenson D. 1995. In *Neptune and Triton*, ed. D Cruikshank, M Matthews, A Schumann, pp. 37–108. Tucson: Univ. Ariz. Press
Luu J, Jewitt D. 1996. Color diversity among the Centaurs and Kuiper belt objects. *Astron. J.* 112:2310–18
Luu J, Marsden BG, Jewitt D, Trujillo CA, Hergenrother CW, et al. 1997. A new dynamical class of object in the outer solar system. *Nature* 387:573–75
Luu JX, Jewitt DC. 1998a. Optical and infrared reflection spectrum of Kuiper belt object 1996-TL66. *Ap. J.* 494:L117–20
Luu JX, Jewitt DC. 1998b. Deep imaging of the Kuiper belt with the Keck 10-m telescope. *Ap. J. Lett.* 502:91–94
Malhotra R. 1995. The origin of Pluto's orbit: implications for the solar system beyond Neptune. *Astron. J.* 110:420–29
Malhotra R. 1996. The phase space structure near Neptune resonances in the Kuiper belt. *Astron. J.* 111:504–16
Malhotra R, Williams JG. 1998. Pluto's heliocentric orbit. In *Pluto and Charon*, ed. SA Stern, D Tholen, pp. 127–57. Tucson: Univ. Ariz. Press
McKinnon WB. 1989. On the origin of the Pluto-Charon binary. *Ap. J. Lett.* 344:41–44
Morbidelli A. 1997. Chaotic diffusion, and the origin of comets from the 3/2 resonance in the Kuiper belt. *Icarus* 127:1–12
Morbidelli A, Valsecchi GB. 1997. Neptune scattered planetesimals could have sculpted the primordial Edgeworth-Kuiper belt. *Icarus* 128:464–68
Moroz LV, Arnold G, Korochantsev AV, Wusch R. 1998. Natural solid bitumens as possible analogs for cometary and asteroid organics: 1. Reflectance spectroscopy of pure Bitumens. *Icarus* 134:253–68
Oort JH. 1950. The structure of the cloud of comets surrounding the solar system and a hypothesis concerning its origin. *Bull. Astron. Inst. Netherlands* 11:91–110
Petit J-M, Morbidelli A, Valsecchi G. 1998. Large scattered planetesimals and the excitation of the small body belts. *Icarus.* In press
Pollack J, Hubickyj O, Bodenheimer P, Lissauer J, Podolak M, Greenzweig Y. 1996. Formation of the giant planets by concurrent accretion of solids and gas. *Icarus* 124:62–85
Russell HN. 1916. On the albedo of the planets and their satellites. *Ap. J.* 43:173–95
Shul'man LM. 1972. The chemical composition of cometary nuclei. In *The Motion, Evolution of Orbits, and Origin of Comets, IAU Symp. 45*, ed. G Chebotarev, E Kazimirchak-Polonskaia, B Marsden. p. 265–70. Dordrecht, The Netherlands: Reidel
Slattery W, Benz W, Cameron A. 1992. Giant impacts on a primitive Uranus. *Icarus* 99:167–74
Stern SA. 1991. On the number of planets in

the solar system: the population of 1000 km bodies. *Icarus* 90:271–81
Stern SA. 1995. Collisional timescales in the kuiper disk and their implications. *Astron. J.* 110:856–68
Stern SA. 1996a. On the collisional environment, accretion time scales, and architecture of the massive, primordial Kuiper belt. *Astron. J.* 112:1203–11
Stern SA, Colwell JE. 1997. Collisional erosion in the primordial Edgeworth-Kuiper belt and the generation of the 30-50 AU Kuiper gap. *Ap. J.* 490:879–82
Tholen D, Buie M. 1997. The orbit of Charon. *Icarus* 125:245–60
Trujillo C, Jewitt DC. 1998. A semi-automated sky survey for slow-moving objects suitable for a Pluto express mission encounter. *Astron. J.* 115:1680–87
Tyson JA, Guhathakurta P, Bernstein G, Hut P. 1992. Limits on the surface density of faint Kuiper belt objects. *Bull. Am. Astron. Soc.* 24:1127
Ward WR, Hahn JH. 1998. Dynamics of the trans-Neptune region: apsidal waves in the Kuiper belt. *Astron. J.* 116:489–98
Weidenschilling S. 1977. The distribution of mass in the planetary system and solar nebula. *Astrophys. Space Sci.* 51:153–58
Whipple FL. 1951. A comet model. I. The acceleration of comet Encke. *Ap. J.* 111:375–94
Whipple FL. 1964. Evidence for a comet belt beyond Neptune. *Proc. Natl. Acad. Sci. USA* 51:711–18
Williams IP, O'Ceallaigh DP, Fitzimmons A, Marsden BG. 1995. The slow moving objects 1993 SB and 1993 SC. *Icarus* 116:180–85
Yamamoto S, Mukai T. 1998. Dust production by impacts of interstellar dust on Edgeworth-Kuiper objects. *Astron. Ap.* 329:785–91